Electronic Supplementary Material (ESI) for RSC Advances.

Supplementary Information

Silver on 2D White-C_3N_4 Support Photocatalyst for Mechanism Insight: Synergetic Utilization of Plasmonic Effect for Solar Hydrogen Evolution

Jianjian Yi[1], Xiaojie She[1], Yanhua Song[2], Hui Xu[*1], Peng Zhang[3], Zhao Mo[1], Liang Liu[1], Daolin Du[1], Huaming Li[*1]

1. School of the Environment and Safety Engineering, Institute for Enetgy Research, Jiangsu University, Zhenjiang 212013, P. R. China

2. School of Environmental and Chemical Engineering, Jiangsu University of Science and Technology, Zhenjiang 212003, P. R. China

3. Institute of Advanced Materials, Jiangsu University, Zhenjiang 212013, P. R. China

***Corresponding author:** Tel.:+86-511-88791800; Fax: +86-511-88791708;
E-mail address: xh@ujs.edu.cn, lihm@ujs.edu.cn

Computational methods.

Spin-polarized DFT calculations were performed using the DMol^3 code.[1,2] The well-known Perdew-Burke-Ernzerhof (PBE) functional with generalized gradient approximation (GGA) is used as the exchange-correlation functional.[3] The core electrons are described by the all electron relativistic (AER) core treat method.[4] The double numerical plus polarization (DNP) is chosen as the atomic orbital basis set.[1] A smearing of 0.005 Ha is applied to the orbital occupation. The convergence tolerances of energy, maximum force and displacement are 1.0×10^{-5} Ha, 0.002 Ha/Å, and 0.005 Å, respectively. The Ag (100) surface is modeled by a p(2×2) cell with seven layer Ag slab. The middle three layers are fixed at their bulk positions and the remaining atoms are allowed to relax fully. For monolayer g-C_3N_4, a orthorhombic supercell is constructed as $7.130 \times 7.130 \times 20.000$ Å^3.

Photocatalytic activity

For photocatalytic degradation experiment, the organic dye methyl orange (MO) was used as a model pollutant. In detail, 15 mg samples were added into 50 ml MO (10 mg/L) in a Pyrex photocatalytic reactor with a circulating water system to maintain a constant temperature (30°C). Before irradiation, the suspensions were magnetically stirred for 30 min in the dark to ensure that MO could reach the absorption-desorption equilibrium on the photocatalyst surface. At certain time intervals, 3 mL aliquots were sampled and centrifuged to remove the photocatalyst particles. Then the filtrates were analyzed by recording variations of the absorption band maximum (464 nm) in the UV-vis spectra of MO using a UV-vis spectrophotometer (UV-2450 Shimadzu). The air velocity was 2 L/min and the photocatalytic reaction was performed under a 300W Xe lamp with a 400 nm cutoff filter.

Characterization.

The transmission electron microscopy (TEM) images were recorded on a JEOL-JEM-2010 (JEOL, Japan) operated at 200 kV. The powder X-ray diffraction (XRD) patterns was recorded using a Bruker D8 diffractometer with Cu Kα radiation (λ = 1.5418 Å) in the range of 2θ = 10-80°. X-ray photoelectron spectroscopy (XPS)

analysis was performed on an ESCALab MKII X-ray photoelectron spectrometer using Mg Kα radiation. The Fourier transform infrared spectra (FT-IR) of the samples were recorded using a Nicolet Nexus 470 spectrometer. Ultraviolet visible (UV-vis) diffuse reflection spectra were measured using a UV-vis spectrophotometer (Shimadzu UV-2450, Japan) in the range of 200-800 nm. $BaSO_4$ was used as a reflectance standard material. The photoluminescence (PL) spectra of the samples were obtained by a QuantaMaster & TimeMaster Spectrofluorometer. Electron spin resonance (ESR) spectra were conducted on a Bruker model ESR JES-FA200 spectrometer.

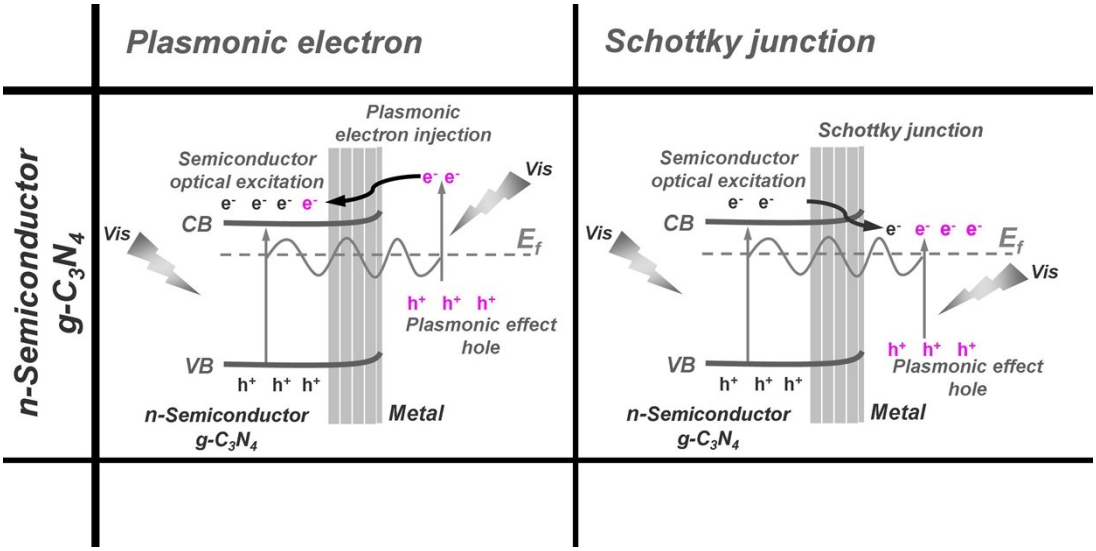

Figure S1. Schematic illustrations for band diagrams illustrating the charge migration driven by the plasmonic effect and Schottky junction in the metal-(n-type) semiconductor (n-type g-C_3N_4), respectively.

Figure S2. Photographs of the bulk g-C_3N_4 and 2D White-C_3N_4.

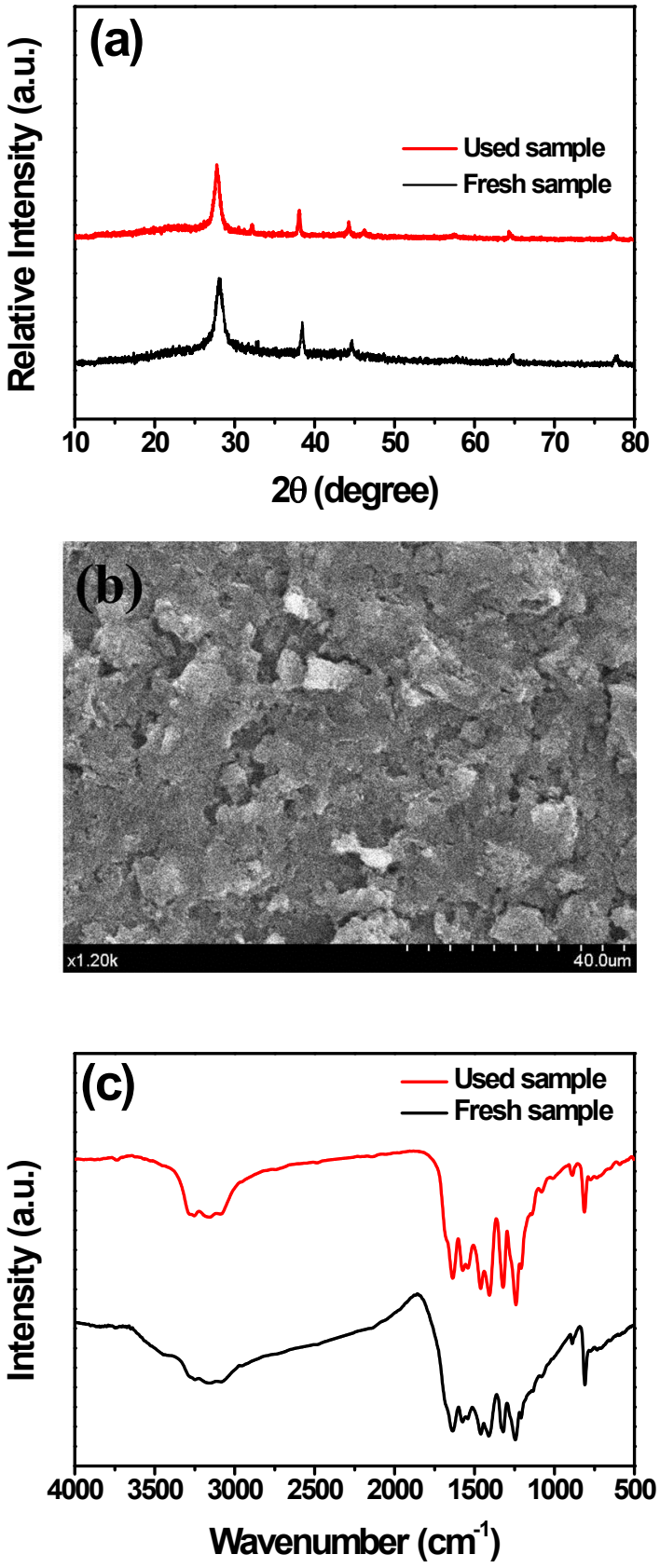

Figure S3. (a) The XRD patterns, (b) SEM image and (c) FT-IR spectra of the used 2% Ag/2D White-C_3N_4 photocatalyst.

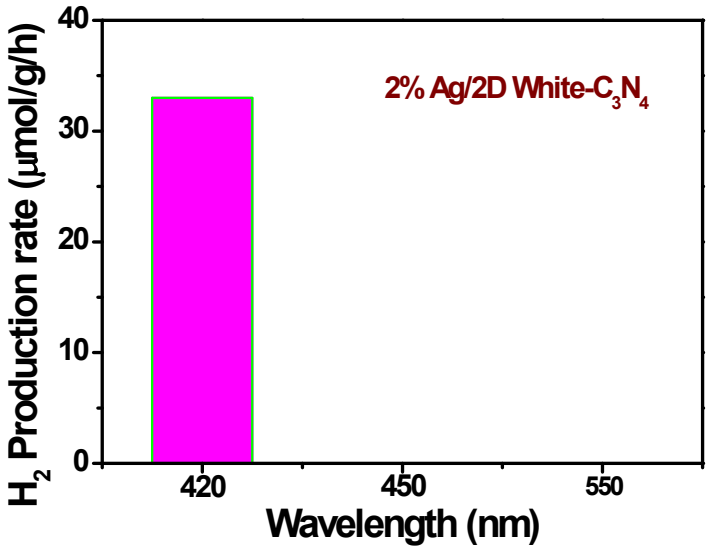

Figure S4. The wavelength-dependent H_2 evolution by using 2% Ag/2D White-C_3N_4.

Figure S4 exhibits the wavelength-dependent H_2 evolution by using 2% Ag/2D White-C_3N_4. When the sample was irradiated under λ=420 nm, the H_2 production rate was ~33.0 μmol/g/L. This value is quite lower than under λ>400 nm irradiation (~354.2 μmol/g/L). The reason why the value decreases sharply is that Ag particles cannot be excited under λ=420 nm. Thus, the hot electrons injection could not work. The H_2 cannot be generated using 2% Ag/2D White-C_3N_4 under the irradiation (λ=450 and 550 nm). For λ = 450 nm irradiation, although metal Ag could be excited, 2D White-C_3N_4 could not. For λ=550 nm, neither metal Ag nor semiconductor 2D White-C_3N_4 could not be excited.

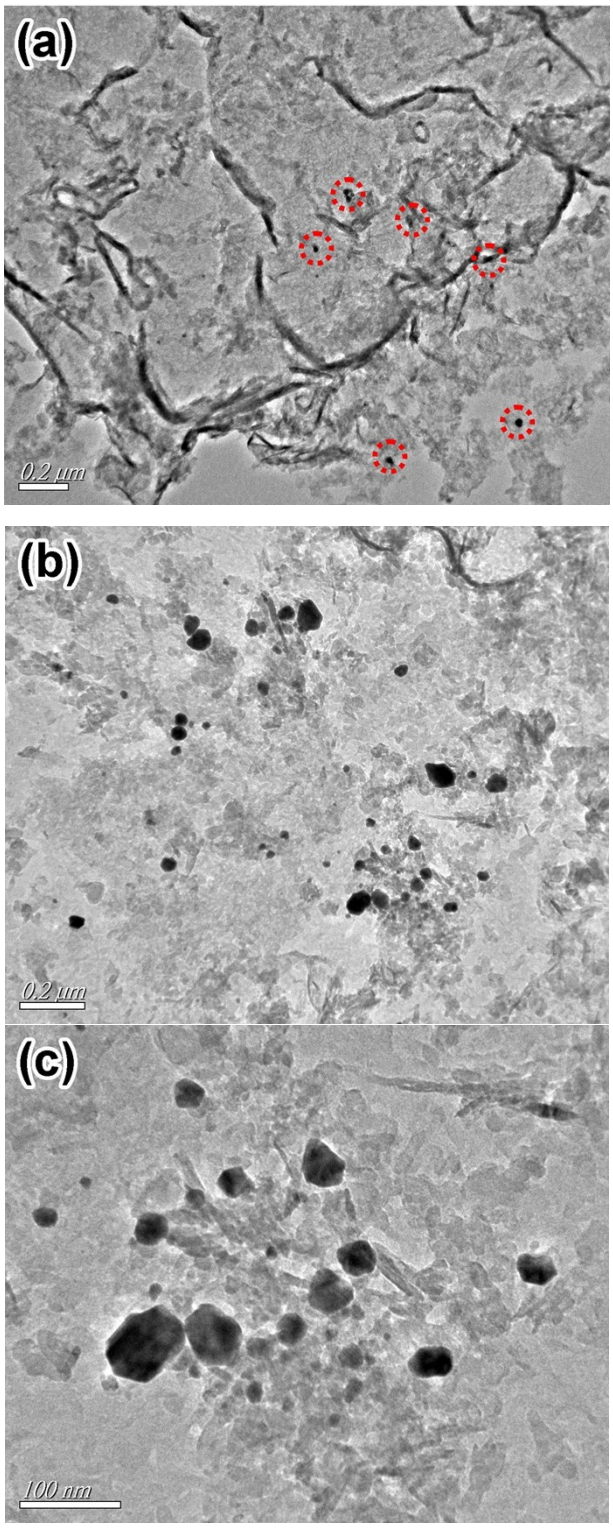
(a)
0.2 μm
(b)
0.2 μm
(c)
100 nm

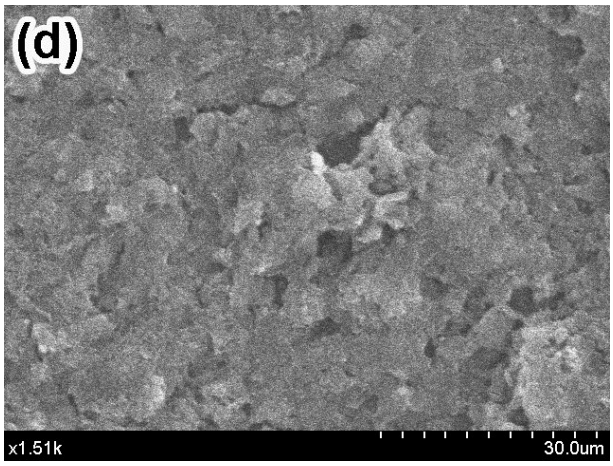

Figure S5. TEM images of (a) 1% Ag/2D White-C_3N_4 and (b and c) 10% Ag/2D White-C_3N_4, (c) SEM image of 2% Ag/2D White-C_3N_4.

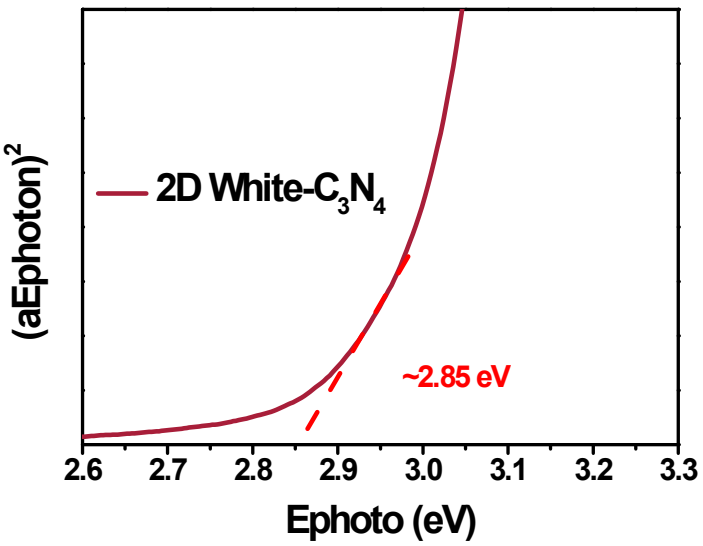

Figure S6. The estimated band gap of 2D White-C_3N_4.

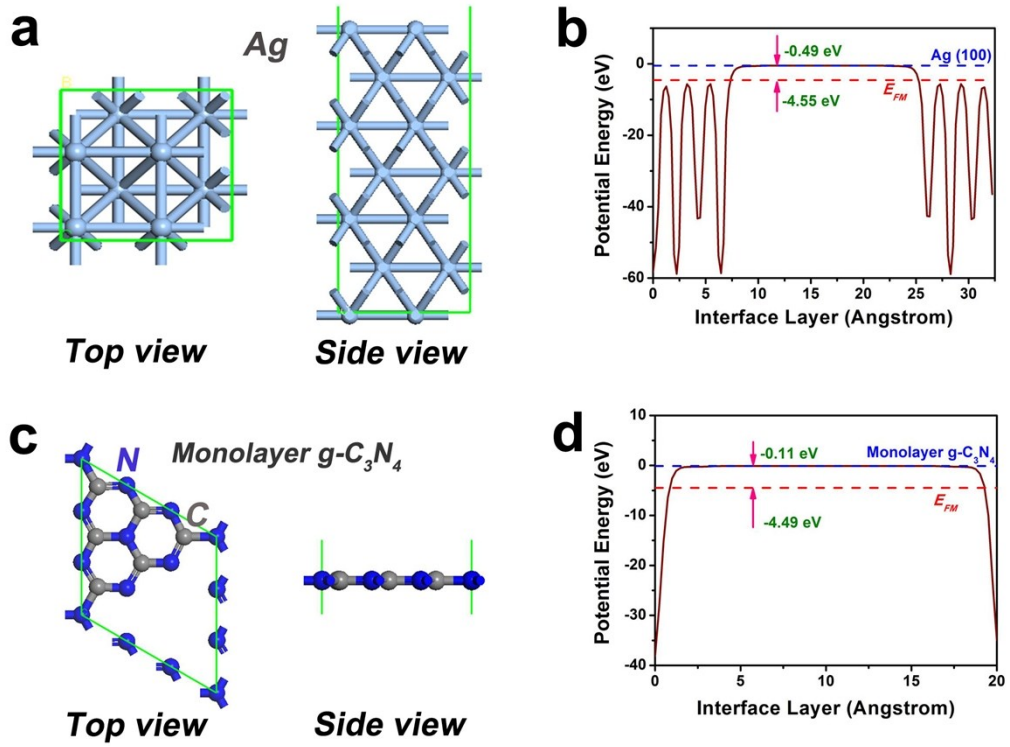

Figure S7. Simulation models of (a) Ag (100) and (c) monolayer g-C_3N_4, the potential diagrams of (b) Ag and (d) monolayer g-C_3N_4.

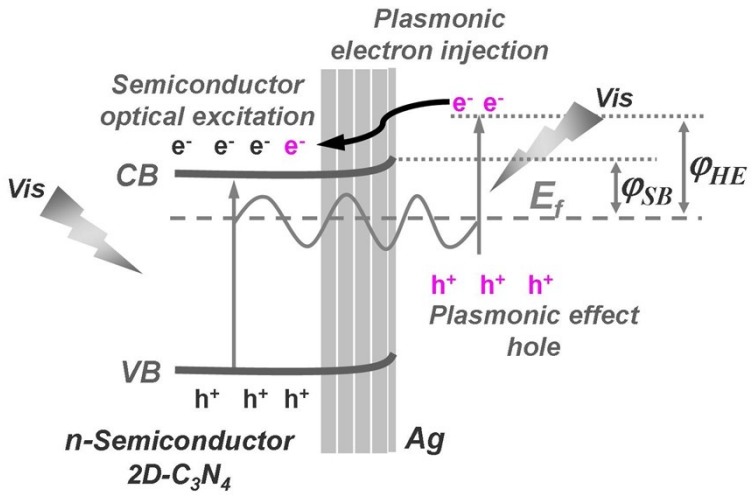

Figure S8. Schematic illustrations for injecting the hot electrons with energies high enough to CB of n-Semiconductor 2D-C_3N_4.

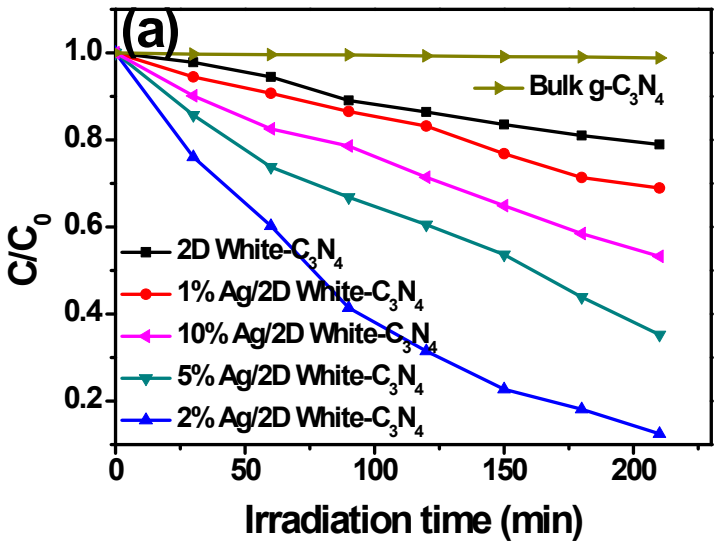
(a)
C/C0
Irradiation time (min)
Bulk g-C3N4
2D White-C3N4
1% Ag/2D White-C3N4
10% Ag/2D White-C3N4
5% Ag/2D White-C3N4
2% Ag/2D White-C3N4

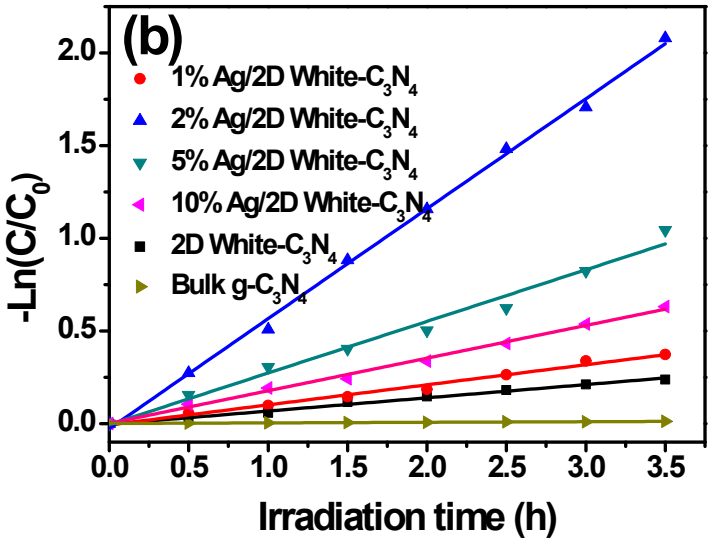
(b)
-Ln(C/C0)
Irradiation time (h)
1% Ag/2D White-C3N4
2% Ag/2D White-C3N4
5% Ag/2D White-C3N4
10% Ag/2D White-C3N4
2D White-C3N4
Bulk g-C3N4

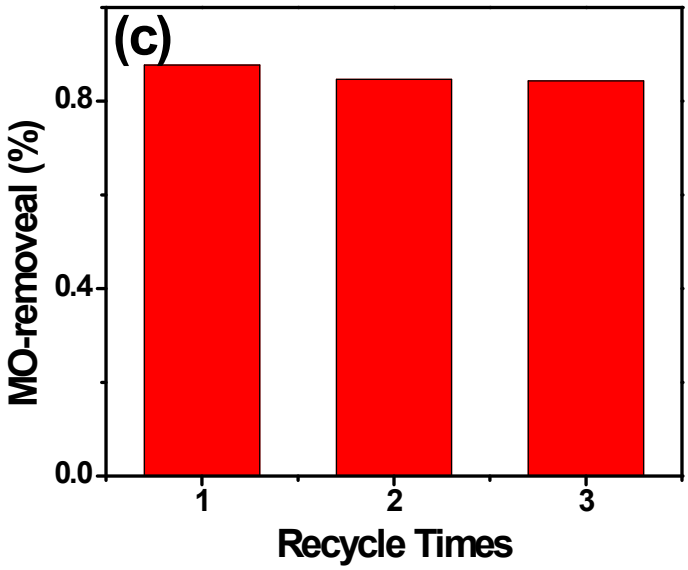

Figure S9. (a) The photocatalytic degradation of MO dye by the 0.015 g photocatalysts under visible light irradiation, (b) the kinetics of MO degradation using the bulk g-C_3N_4, 2D White-C_3N_4 and Ag/2D White-C_3N_4 under visible light irradiation, and (c) stability test of 2% Ag/2D White-C_3N_4 for MO degradation under visible light irradiation.

Figure S9a shows the photocatalytic avtivities of the samples for degradation of MO under visible light irradiation. Obviously, after 3.5 h visible light irradiation, the photodegradation activity of the bulk g-C_3N_4 was negligible for MO. And ~21% MO could be removed by 2D White-C_3N_4, which indicates that 2D structure is good for enhancing photocatalytic activity. When Ag was introduced into 2D White-C_3N_4 nanosheet, the photodegradation activities of the samples were obviously improved. The 2% Ag/2D White-C_3N_4 showed the best photodegradation activity. After 3.5 h visible light irradiation, it had ~66% improvement, in comparison to 2D White-C_3N_4. It is evident that 2D ultrathin structure and introduction of Ag are very significant for improving photocatalytic activity. The photodegradation activities of the samples correspond directly with photocatalytic H_2 evolution well. To understand the process of the photocatalysis reaction, the photodegradation kinetics of MO under visible light irradiation was analyzed. From **Figure S9b**, the linear relationship of -Ln(C/C_0) versus time follows first-order reaction dynamics under the experimental conditions.

C and C_0 is the MO concentrations at time 0 and *t*, respectively. The kinetic constant (*k*) and regression coefficient (R^2) were calculated and given in **Table S1**, which can be found that 2% Ag/2D White-C_3N_4 has the maximum apparent rate of 0.5934 h^{-1}, which is ~185 and 8 times higher than that of the bulk g-C_3N_4 (0.0032 h^{-1}) and 2D White-C_3N_4 (0.0714 h^{-1}), respectively. In addition, the result in **Figure S9c** indicated that after 3 cycles, the photodegradation activity of 2% Ag/2D White-C_3N_4 only reduced a little, which could be ascribed to the loss of the sample during the experiments.

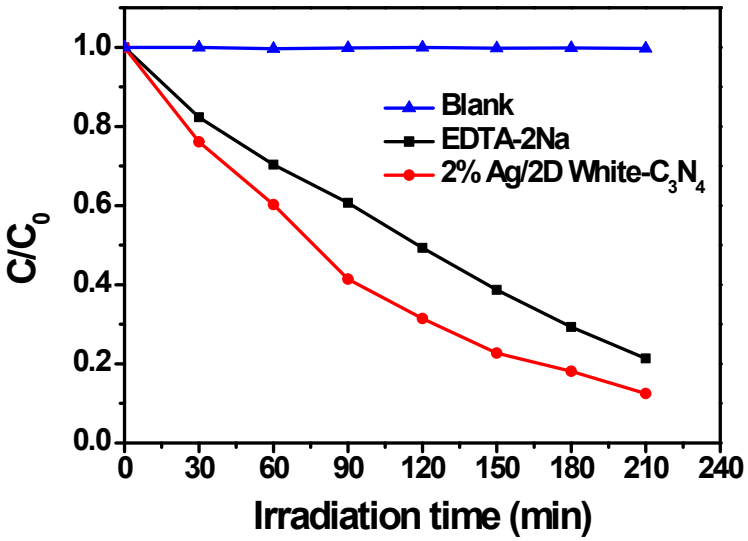

Figure S10. Comparison of photocatalytic activities of 2% Ag/2D White-C_3N_4 composite for the degradation of MO with or without adding EDTA-2Na under visible light irradiation.

The hole trapping experiment was carried out through adding the scavenger disodium ethylenediaminetetra acetate (EDTA-2Na) (**Figure S10**). Obviously, when EDTA-2Na was added, the degradation efficiency was inhibited. These results indicate that the holes and $O_2^{\bullet-}$ play a role in photodegradation process and $O_2^{\bullet-}$ is the main active species. For photodegradation reaction, when Ag/2D White-C_3N_4 is irradiated by visible light, O_2 can be reduced into $O_2^{\bullet-}$ with oxidize ability. These $O_2^{\bullet-}$ and photogenerated holes can oxidize organic pollutant (MO) (**Figure S10b)**. These cycles continue to happen, so photocatalytic reaction proceeds for both hydrogen evolution and photodegradation reaction.

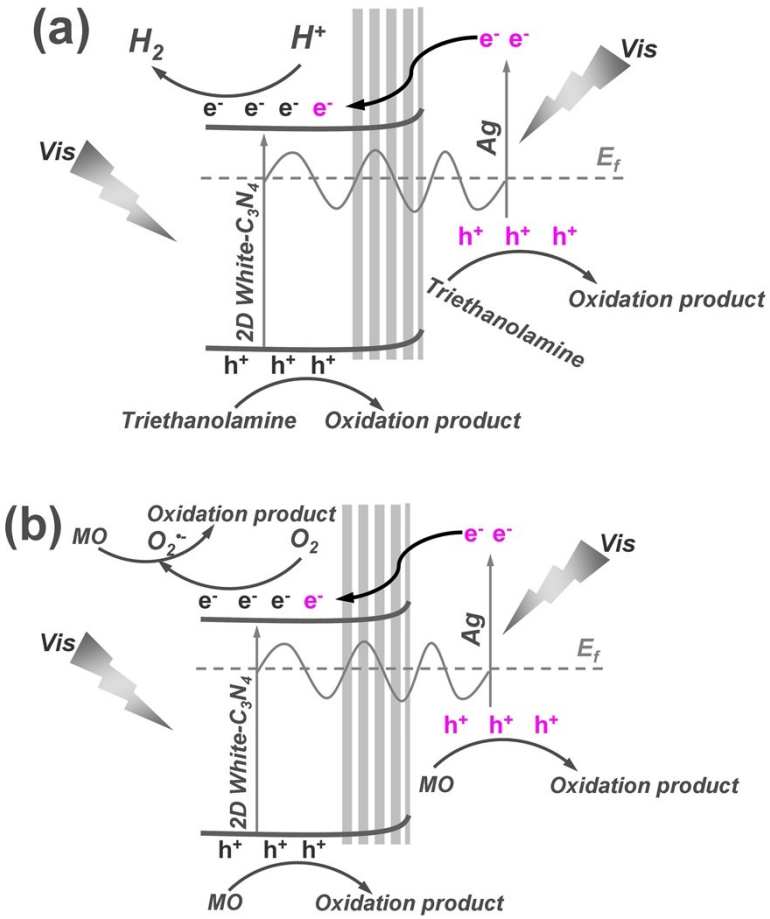

Figure S11. (a) and (b) Schematic illustration of proposed mechanism for the photocatalytic H_2 evolution and the degradation of the pollutant by synergetic utilization plasmonic effect.

Table S1. Kinetic constants and regression coefficients of MO degradation under visible light irradiation.

Photocatalysts	Kinetic constant (k (h^{-1}))	R^2
Bulk g-C_3N_4	0.0032	0.9845
2D White-C_3N_4	0.0714	0.9879
1% Ag/2D White-C_3N_4	0.1082	0.9879
2% Ag/2D White-C_3N_4	0.5934	0.9974
5% Ag/2D White-C_3N_4	0.2786	0.9802
10% Ag/2D White-C_3N_4	0.1761	0.9943

Table S2 shows the BET surface area and pore volume of as-prepared samples. The BET surface areas of Ag/2D White-C_3N_4 composites exhibit a gradual decrease with the increase of the content of Ag, which is due to the introduction of Ag. The photocatalytic activity of 2D white-C_3N_4 is greatly increased, as its surface area is obviously increased compared with that of the bulk g-C_3N_4. Although, the surface areas of the composites is decreased with the comparison of that of 2D White-C_3N_4, the photocatalytic avtivities of the composites are greatly increased.

Table S2. BET surface area and pore volume of as-prepared samples.

Sample	BET surface area [m^2/g]	Pore volume [cm^{-3}/g]
Bulk g-C_3N_4	5.38	48.80
2D White-C_3N_4	264.70	48.61
1% Ag/2D White-C_3N_4	190.64	46.72
2% Ag/2D White-C_3N_4	183.94	46.63
5% Ag/2D White-C_3N_4	159.85	45.71
10% Ag/2D White-C_3N_4	120.56	44.92

References:

1. B. Delley, *J. Chem. Phys.*, 1990, **92**, 508.

2. B. Delley, *J. Chem. Phys.*, 2000, **113**, 7756.

3. J. P. Perdew, K. Burke, M. Ernzerhof, *Phys. Rev. Lett.*, 1996, **77**, 3865.

4. D. D. Koelling, B. N. Harmon, *J. Phys. C: Solid State Phys.*, 1977, **10**, 3107.